

# WATER MASERS IN THE ANDROMEDA GALAXY: I. A SURVEY FOR WATER MASERS, AMMONIA, AND HYDROGEN RECOMBINATION LINES

JEREMY DARLING, BENJAMIN GERARD<sup>1</sup>, NIKTA AMIRI<sup>2</sup>, & KELSEY LAWRENCE

Center for Astrophysics and Space Astronomy, Department of Astrophysical and Planetary Sciences, University of Colorado, 389 UCB, Boulder, CO 80309-0389, USA

<sup>1</sup>Current address: University of Victoria, Department of Physics and Astronomy, 3800 Finnerty Rd., Victoria, V8P 5C2, Canada

## ABSTRACT

We report the results of a Green Bank Telescope survey for water masers, ammonia (1,1) and (2,2), and the H66 $\alpha$  recombination line toward 506 luminous compact 24  $\mu$ m-emitting regions in the Andromeda Galaxy (M31). We include the 206 sources observed in the Darling (2011) water maser survey for completeness. The survey was sensitive enough to detect any maser useful for  $\sim 10 \mu$ as yr<sup>-1</sup> astrometry. No new water masers, ammonia lines, or H66 $\alpha$  recombination lines were detected individually or in spectral stacks reaching rms noise levels of  $\sim 3$  mJy and  $\sim 0.2$  mJy, respectively, in 3.1–3.3 km s<sup>-1</sup> channels. The lack of detections in individual spectra and in the spectral stacks is consistent with Galactic extrapolations. Contrary to previous assertions, there do not seem to be additional bright water masers to be found in M31. The strong variability of water masers may enable new maser detections in the future, but variability may also limit the astrometric utility of known (or future) masers since flaring masers must also fade.

*Keywords:* galaxies: individual (M31) — galaxies: ISM — ISM: molecules — Local Group — masers — radio lines: galaxies

## 1. INTRODUCTION

The dominant galaxies in the Local Group, the Milky Way and the Andromeda galaxy (M31), are likely to merge in  $5.86^{+1.61}_{-0.72}$  Gyr (van der Marel et al. 2012b). The key quantity for this prediction is the transverse velocity of M31 with respect to the Galaxy. Sohn et al. (2012) and van der Marel et al. (2012a) used *Hubble Space Telescope* observations of thousands of M31 stars referenced to hundreds of compact background galaxies in three fields (near the major and minor axes and in the Giant Southern Stream) over five to seven years to constrain the tangential velocity of M31 to  $\leq 34.3$  km s<sup>-1</sup> ( $1\sigma$ ). The consistency of the M31-Milky Way velocity with a radial orbit, infalling at  $-109.3 \pm 4.4$  km s<sup>-1</sup> (van der Marel et al. 2012a), provides a new estimate of the Local Group timing mass to be  $(4.93 \pm 1.63) \times 10^{12} M_{\odot}$  (van der Marel et al. 2012a), although van der Marel et al. (2012a) derive a best estimate of  $(3.17 \pm 0.57) \times 10^{12} M_{\odot}$ , citing cosmic variance as an uncertainty floor on the timing argument estimation of the Local Group mass. The transverse velocity of M31 is thus essential to our understanding of the Local Group’s future (and past) dynamical evolution as well as the density profiles and distribution of dark matter halos (Peebles

et al. 2001; Loeb et al. 2005; Reid et al. 2010).

The Sohn et al. (2012) and van der Marel et al. (2012a,b) results can be independently verified and possibly refined using maser proper motions in M31. Molecular masers, while small in number, are compact high brightness temperature light sources arising in the molecular ring of M31 that provide  $\sim 10$  microarcsecond ( $\mu$ as) astrometry using Very Long Baseline Interferometry (VLBI). Brunthaler et al. (2005, 2007) have measured the proper motions of Galactic analog 22 GHz water (H<sub>2</sub>O) masers discovered in M31’s satellite galaxies M33 (first by Churchwell et al. 1977) and IC 10 (Henkel, Wouterloot, & Bally 1986), obtaining their 3-dimensional velocities with respect to the Milky Way. Brunthaler et al. (2005) also measured the proper rotation of M33, which provides a geometric determination of its distance via “rotational parallax.” The same can be done with masers in M31 (Darling 2011).

Detecting Galactic analog masers of any type in M31 is challenging, due to its distance and large angular size. The M31 distance reduces Galactic maser flux densities by a factor of  $\sim 10^4$ , so only the brightest Galactic masers could be detected in M31, provided that surveys are sensitive to  $\sim 10$  mJy spectral lines (Darling 2011). The large angular size of M31 — the molecular ring is roughly  $2^{\circ} \times 0.5^{\circ}$  — implies that surveys for masers, particularly H<sub>2</sub>O, need to be pointed in order to reach adequate sensitivity. New radio telescope

jdarling@colorado.edu

<sup>2</sup>Current address: Jet Propulsion Laboratory, M/S 238-600, 4800 Oak Grove Dr., Pasadena, CA 91109, USA

facilities with larger collecting areas or larger fields of view than are currently available may improve this situation.

Sullivan (1973) may have made the first search for H<sub>2</sub>O masers in M31, making no detections toward the nucleus and “emission nebula #132.” Greenhill et al. (1995) and Imai et al. (2001) report pointed H<sub>2</sub>O maser surveys toward H II regions in M31, reaching 1 $\sigma$  rms noise levels of 29 and 70 mJy, respectively. Claussen & Beasley (private communication) surveyed the nuclear region and most of the molecular ring using the Very Large Array, making no H<sub>2</sub>O maser detections and reaching an rms noise of 30 mJy per beam. Sjouwerman et al. (2010) detected the first maser of any type in M31, a Class II methanol (CH<sub>3</sub>OH) maser at 6.7 GHz, but no associated water maser was detected (see also Darling 2011, and this work). Finally, Darling (2011) conducted a survey of 206 compact 24  $\mu$ m sources in the molecular ring with  $\sim$ 3 mJy rms noise per 3.3 km s<sup>-1</sup> channel and detected five water masers. The water maser non-detections prior to 2011 were all consistent with the aggregate star formation rate of M31, and these surveys were not sufficiently sensitive to detect a typical Galactic maser at the distance of M31 (Bruntz et al. 2006). The historical lack of Galactic analog water maser detections in M31 has simply been a problem of sensitivity and of locating likely sites of maser activity, both of which now have remedies.

In this paper, we describe an extension of the Darling (2011) Green Bank Telescope<sup>1</sup> (GBT) H<sub>2</sub>O maser survey to include an additional 300 unresolved 24  $\mu$ m sources in M31. We also report on the simultaneous observation of two ammonia (NH<sub>3</sub>) lines and one hydrogen radio recombination line (H66 $\alpha$ ) toward all 506 locations in the combined surveys. In a companion paper, we examine the physical conditions most likely to produce detectable H<sub>2</sub>O maser emission in M31 (Amiri & Darling 2016, Paper II).

Throughout this manuscript, we use heliocentric velocities (optical definition) and assume the following about M31: a systemic velocity of  $-300$  km s<sup>-1</sup> (de Vaucouleurs et al. 1991), a distance of 780 kpc (McConnachie et al. 2005), and central coordinates 00:42:44.3, +41:16:09 (J2000).

## 2. SAMPLE SELECTION

A Spitzer 24  $\mu$ m map of M31 (Gordon et al. 2008) guided the GBT observations in two important ways: source selection and completeness. The association of water masers with (ultra)compact H II regions is well known, but the molecular gas as traced by optically thick CO emission does not necessarily indicate these regions. Likewise, H $\alpha$ -selected H II regions may select *against* dust-enshrouded ultra-compact H II

regions (but see Amiri & Darling 2016). Compact 24  $\mu$ m emission, however, is a good indicator of likely sites of H<sub>2</sub>O maser emission, and there is a rough relationship between far-IR emission and water maser luminosity (Jaffe et al. 1981; Urquhart et al. 2011, although the latter relies on bolometric luminosities). We therefore selected compact 24  $\mu$ m sources associated with the dusty molecular — and presumably star-forming — regions in M31 (“compact” means unresolved at the 23.5 pc resolution of the Spitzer map). This method can also, however, select objects unlikely to produce water masers, such as planetary nebulae, giant stars, and background galaxies.

We constructed a catalog of 506 unresolved 24  $\mu$ m sources working from the brightest down to the point where most of the 24  $\mu$ m emission becomes extended, about 4 MJy steradian<sup>-1</sup> at peak specific intensity. Although this pointed survey does not include all star formation in M31, it does include the majority of likely locations for strong H<sub>2</sub>O maser activity. By working down in luminosity through the catalog of compact 24  $\mu$ m sources, we have surveyed a large fraction of the total ongoing star formation in the galaxy (e.g., Tabatabaei & Berkhuijsen 2010; Ford et al. 2013) and thus most of the likely H<sub>2</sub>O-bearing regions (Amiri & Darling 2016). Figure 1 shows the 24  $\mu$ m map of M31 with the 506 pointing centers and primary beam size for our GBT water maser survey, including the masers detected by Darling (2011).

## 3. OBSERVATIONS AND DATA REDUCTION

Darling (2011) observed 206 24  $\mu$ m sources in M31 using the GBT in 2010 October through December. The 6<sub>16</sub>–5<sub>23</sub> 22.23508 GHz ortho-water maser line observations were reported in Darling (2011), but simultaneous observations of the para-ammonia (NH<sub>3</sub>) rotational ground state inversion transitions in the metastable states ( $J, K$ ) = (1, 1) and (2, 2) at 23.6945 and 23.72263 GHz and the hydrogen recombination line H66 $\alpha$  at 22.36417 GHz were not. We subsequently observed all four of these lines toward an additional 300 24  $\mu$ m sources in 2011 October through 2012 January. The telescope configuration was identical to that described by Darling (2011): A 632–674 km s<sup>-1</sup> (50 MHz) bandpass was centered, for each of the four observed transitions, on a heliocentric velocity of  $-300$  km s<sup>-1</sup> for 239 sources in the central parts of the galaxy and along the minor axis, on  $-100$  km s<sup>-1</sup> for 136 sources in the redshifted northeast wedge of the galaxy, and on  $-500$  km s<sup>-1</sup> for 131 sources in the blueshifted southwest wedge of the galaxy (Figure 1 and Table 1).

<sup>1</sup> The National Radio Astronomy Observatory is a facility of the National Science Foundation operated under cooperative agreement by Associated

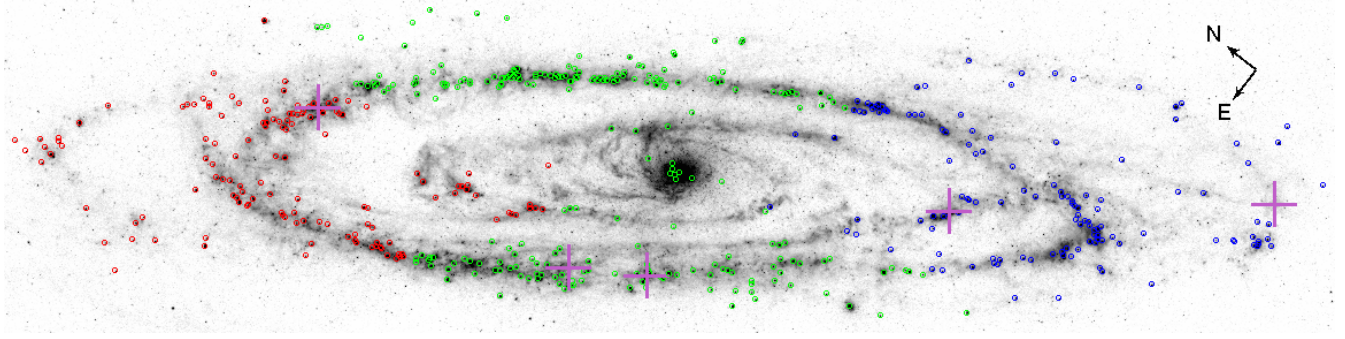


**Figure 1.** Spitzer 24  $\mu\text{m}$  map of M31 (Gordon et al. 2008). The circles indicate the 506 pointing centers (the circles are to scale, showing the 33'' FWHM beam). Crosses mark the masers detected by Darling (2011) and are enlarged for clarity. Colors indicate the systemic (green), red, and blue spectrometer tuning centers at  $-300$ ,  $-100$ , and  $-500$   $\text{km s}^{-1}$ , respectively. The image spans  $2.5^\circ \times 0.6^\circ$ .

**Table 1.** M31 Line Survey Results

Object (J2000)	H <sub>2</sub> O (mJy)	NH <sub>3</sub> (1,1) (mJy)	NH <sub>3</sub> (2,2) (mJy)	H66 $\alpha$ (mJy)	V <sub>obs</sub> (km s <sup>-1</sup> )	V <sub>CO</sub> (km s <sup>-1</sup> )	Object (J2000)	H <sub>2</sub> O (mJy)	NH <sub>3</sub> (1,1) (mJy)	NH <sub>3</sub> (2,2) (mJy)	H66 $\alpha$ (mJy)	V <sub>obs</sub> (km s <sup>-1</sup> )	V <sub>CO</sub> (km s <sup>-1</sup> )
003838.7+402613.5 <sup>a</sup>	2.0	2.4	2.3	2.2	-500	...	003849.2+402551.7 <sup>a</sup>	3.2	2.7	2.6	3.2	-500	...
003852.5+401904.9	2.0	2.1	2.4	2.0	-500	...	003904.8+402927.4	1.2	1.3	1.5	1.3	-500	...
003906.7+403704.5	3.5	2.8	3.0	3.0	-500	...	003909.8+402705.0	2.1	2.1	2.1	2.0	-500	...
003910.2+403725.6	3.2	2.8	4.2	2.9	-500	...	003914.6+404157.9	2.1	2.2	2.3	2.1	-500	...
003916.1+403629.5	3.0	2.6	2.8	2.9	-500	...	<b>003918.9+402158.4</b>	0.7	0.6	0.6	0.5	-500	...
003930.2+402106.4	3.7	2.6	3.0	3.5	-500	...	003933.2+402215.6	3.2	2.8	2.8	3.2	-500	...
003935.2+404814.6	2.1	2.1	2.1	2.2	-500	...	003937.5+402011.5	3.4	2.9	2.9	3.2	-500	...
003938.9+401921.3	2.5	2.3	2.4	2.4	-500	...	003939.1+405018.3	1.9	2.3	2.0	2.0	-500	...
003939.8+402856.3	3.1	2.8	2.8	3.1	-500	...	003941.5+402133.7	1.7	2.1	2.2	2.3	-500	...
003941.9+402045.6	2.0	2.0	2.1	2.1	-500	...	003943.0+402039.9	2.1	2.4	2.5	2.3	-500	...
003944.5+402030.4	3.3	2.9	2.5	2.6	-500	...	003945.2+402058.0	1.9	2.4	2.4	2.2	-500	...
003948.5+403113.1	2.0	1.9	2.0	2.2	-500	...	003950.5+402305.9	2.2	2.2	2.2	2.2	-500	...
003950.9+402252.1 <sup>b</sup>	1.9	2.1	2.2	2.0	-500	...	003951.3+405306.1	1.9	2.1	2.1	2.2	-500	...
003954.4+403820.4 <sup>a</sup>	3.4	3.5	3.6	3.6	-500	...	003956.8+402437.6	1.9	2.2	2.4	2.1	-500	...
004000.3+405318.6	2.0	2.2	2.2	2.1	-500	...	004004.7+405840.9	3.2	3.2	3.2	3.3	-500	...
004010.4+404517.7	1.9	2.0	2.3	2.0	-500	-513	004020.3+403124.5	2.1	2.4	2.6	2.0	-500	...
004020.5+403723.9	2.0	2.3	2.2	2.1	-500	-528	004023.8+403904.4	3.4	3.5	3.7	3.3	-500	-495
004026.2+403706.5	3.0	3.7	3.9	3.3	-500	...	004030.9+404230.0	3.0	2.3	2.8	3.1	-500	-466
004031.2+403952.0	2.9	2.4	2.4	2.5	-500	...	004031.3+404032.8	2.1	2.0	2.0	1.6	-500	-453
004031.7+404127.0	3.3	3.0	3.3	2.7	-500	-565	004032.5+405127.4	2.0	2.3	1.9	1.9	-500	-454
004032.6+403856.1	3.3	2.9	2.8	2.6	-500	-558	004032.7+403531.2	2.1	2.4	2.7	2.0	-500	-538
004032.7+403936.5	3.5	3.4	3.4	3.4	-500	-567	004032.7+410045.1	2.0	2.0	2.0	2.1	-500	...
004032.8+405540.2	1.9	2.1	2.2	2.0	-500	-454	004032.9+403919.2	3.3	3.6	3.6	3.2	-500	-565
004033.0+404102.8	3.0	3.7	3.5	3.1	-500	-576	004033.3+403352.1	3.1	2.8	2.7	2.9	-500	...
004033.8+403246.6	3.1	2.8	2.7	2.8	-500	...	004034.7+403541.2	2.8	2.8	3.0	2.8	-500	-582
004035.1+403701.1	4.0	3.5	4.0	3.0	-500	-510	004035.8+403724.6	3.6	5.1	3.3	3.7	-500	...
004036.0+403821.0	3.0	3.3	3.4	3.1	-500	...	004036.1+410117.5	2.1	1.9	1.8	2.0	-500	...
004036.3+403641.9	2.1	2.1	2.2	2.0	-500	-532	004036.3+405329.3	1.9	2.0	2.1	2.1	-500	-575
004036.8+403557.1	2.0	2.2	2.1	2.0	-500	-549	004038.0+403514.9	2.9	3.8	3.3	3.4	-500	-540
004038.0+404728.3	2.0	2.2	2.1	2.0	-500	...	004038.6+403814.7	2.9	3.7	3.6	3.3	-500	...
004038.7+403533.2	2.3	2.2	2.3	2.3	-500	-541	004038.8+403431.0	3.4	3.5	3.3	3.0	-500	-504
004039.4+403730.5	3.4	4.4	3.2	3.3	-500	-547	004039.7+403457.9	2.2	2.2	2.2	2.3	-500	-525
004040.4+402709.8 <sup>b</sup>	2.2	2.2	2.2	2.0	-500	...	004041.6+405105.0	2.0	2.0	1.8	1.7	-500	...
004042.1+403454.5	3.4	3.2	3.5	3.3	-500	-535	004043.3+404321.9	3.1	3.0	2.9	2.7	-500	-533

Table 1 continued

Table 1 (*continued*)

Object	H <sub>2</sub> O	NH <sub>3</sub>	NH <sub>3</sub>	H66 $\alpha$	V <sub>obs</sub>	V <sub>CO</sub>	Object	H <sub>2</sub> O	NH <sub>3</sub>	NH <sub>3</sub>	H66 $\alpha$	V <sub>obs</sub>	V <sub>CO</sub>
(J2000)	(mJy)	(1,1)	(2,2)	(mJy)	(km s <sup>-1</sup> )	(km s <sup>-1</sup> )	(J2000)	(mJy)	(1,1)	(2,2)	(mJy)	(km s <sup>-1</sup> )	(km s <sup>-1</sup> )
004043.6+403530.5	3.3	2.9	2.8	3.2	-500	-552	004043.7+405251.5	2.0	2.0	2.2	2.1	-500	-445
004044.2+404446.4	3.0	2.8	3.1	2.5	-500	...	004045.7+405134.5	1.9	1.8	2.2	1.8	-500	...
004046.4+405541.9	3.0	2.7	2.5	2.6	-500	-519	004046.5+405606.4	2.8	2.7	2.5	2.8	-500	-544
004047.3+405903.2	2.0	2.0	2.1	2.0	-500	-497	004050.0+405938.5	1.7	2.3	2.2	2.0	-500	-502
004051.6+410006.5	2.9	2.5	2.5	2.5	-500	-503	004051.7+403602.3	2.1	2.2	2.3	2.2	-500	...
004051.9+403249.7	3.4	3.8	3.4	2.9	-500	...	004053.0+403218.0	3.8	3.8	3.5	3.7	-500	-480
004055.1+403703.2	3.8	4.0	3.6	3.4	-500	-530	004057.3+403607.0	2.2	2.3	2.4	2.2	-500	...
004058.2+410302.3	1.9	2.2	2.0	2.1	-500	-476	004058.3+403711.1	2.1	2.2	2.1	2.1	-500	-510
004058.4+405325.2	2.2	2.3	2.4	2.0	-500	...	004058.4+410217.9	1.9	2.2	2.1	1.9	-500	-473
004058.4+410225.9	2.0	2.1	2.0	2.1	-500	-474	004058.6+404558.0	2.1	2.0	1.8	2.1	-500	-506
004058.6+410332.3	3.0	2.8	3.0	3.1	-500	-466	004059.1+410233.1	2.1	2.4	2.3	2.2	-500	-477
004059.8+403652.4	4.8	4.2	3.3	3.0	-500	-497	004100.6+410334.0	3.7	3.0	3.0	3.2	-500	-461
004101.6+410405.8	2.3	2.2	2.1	2.1	-500	-457	004102.0+410254.9	1.7	1.9	1.9	1.9	-500	-480
004102.3+410431.7	2.1	2.4	2.2	2.0	-500	-449	004102.7+410344.5	2.1	2.1	2.4	1.9	-500	-456
004103.1+403749.9	2.3	2.4	2.3	2.0	-500	-502	004104.8+410534.6	1.8	1.2	1.2	1.3	-500	-458
004107.2+410410.0	2.0	2.1	2.2	2.2	-500	-459	004107.6+404812.5	3.5	2.9	2.8	3.0	-500	-526
004108.6+410437.9	1.2	1.3	1.2	1.2	-500	-452	004109.1+404852.7	3.0	3.6	3.9	3.4	-500	-490
004109.2+404910.3	3.1	3.6	3.7	3.3	-500	-518	004110.4+404949.5	3.1	3.0	3.5	3.0	-500	-555
004110.6+410516.4	2.2	2.6	2.2	2.2	-500	-450	004112.5+410609.7	3.4	2.6	2.9	2.5	-300	-435
004113.7+403918.6	2.2	2.2	2.3	2.2	-500	-477	004113.8+410814.6	2.0	2.1	2.2	2.0	-300	-422
004113.9+410736.1	2.2	2.0	2.2	2.0	-300	-431	004114.8+410923.7	3.8	3.0	3.3	3.4	-300	-413
004115.9+404011.6	3.1	2.8	2.6	2.7	-500	-448	004119.1+404857.4	3.6	3.1	3.2	3.4	-500	-473
004119.5+411948.8	3.9	3.3	3.1	3.0	-300	...	004120.0+410821.5	3.0	2.7	2.8	2.6	-300	...
004120.9+403414.0	2.4	2.7	2.6	2.5	-500	...	004121.2+411947.8	2.5	2.7	2.5	2.5	-300	...
<b>004121.7+404947.7</b>	1.4	1.5	1.6	1.4	-500	-520	004123.2+405000.6	3.4	3.3	2.9	3.0	-500	-518
004124.1+411124.1	3.1	3.7	3.7	3.7	-300	-398	004124.8+411154.6	3.4	2.9	2.7	2.6	-300	-407
004125.4+404200.4	3.7	3.2	3.1	3.3	-500	-448	004126.1+404959.1	3.7	3.2	3.3	3.5	-500	-502
004126.5+411206.9	3.0	3.0	2.8	2.8	-300	-400	004127.3+404242.7	2.0	2.3	2.3	2.2	-500	-443
004128.1+404155.2	2.0	2.4	2.1	2.2	-500	-462	004128.1+411222.6	3.6	4.0	4.4	3.2	-300	-389
004129.2+411242.8	4.2	4.2	4.1	3.6	-300	-417	004129.3+404218.9	2.2	2.3	2.2	2.2	-500	-440
004129.5+411006.3	4.0	3.9	4.4	3.8	-300	...	004129.8+405059.5	2.2	1.6	1.7	1.7	-500	-463
004129.8+412211.1 <sup>a</sup>	3.1	3.0	2.8	2.9	-300	...	004130.3+410501.7	3.1	3.0	3.4	3.1	-500	-477
004131.9+411331.5	3.8	4.4	4.1	4.1	-300	-401	004135.7+405009.3	2.4	2.8	2.8	2.4	-500	...
004136.9+403805.6	2.2	2.4	2.2	2.3	-500	...	004137.0+405142.5	3.3	3.3	3.0	3.5	-500	-432
004138.6+404401.2	3.4	3.1	3.0	3.1	-500	-426	004141.3+411916.7	2.4	2.3	2.6	2.5	-300	...
004143.6+410840.1	2.0	2.0	2.1	2.0	-500	-404	004144.6+411658.1	3.9	4.4	4.1	3.9	-300	-365
004145.0+404746.4	2.2	2.5	2.4	2.4	-500	...	004146.7+411846.6	3.3	2.8	3.1	3.0	-300	-308
004147.4+411942.4	3.9	4.3	4.4	4.1	-300	-359	004148.2+411903.8	3.6	3.2	4.5	3.1	-300	-358
004149.6+411953.8	2.4	2.7	2.5	2.3	-300	-387	004151.3+412500.7	2.8	2.6	2.7	2.4	-300	...
004151.6+404620.5	2.0	2.4	2.1	2.1	-500	...	004151.9+412442.1	3.3	3.1	3.3	3.6	-300	...
004154.5+404718.9	2.2	2.3	2.2	2.1	-500	-414	004159.4+405720.8	2.1	1.7	1.7	1.8	-500	...
004200.6+404747.8	2.2	2.5	2.4	2.3	-300	...	004200.9+405217.2	2.1	2.2	2.2	2.1	-500	-407
004201.5+404115.7 <sup>a</sup>	2.3	2.4	2.5	2.3	-300	...	004202.4+412436.0	1.1	1.1	1.2	1.3	-300	-323
004202.9+412232.4	1.1	1.3	1.2	1.1	-300	-353	004203.9+404907.1	2.6	2.1	2.1	2.4	-300	...
004204.9+404936.6	2.2	2.4	2.2	2.5	-300	...	004206.7+405621.5	2.0	2.3	2.0	2.0	-500	...
004208.5+405720.2	2.0	2.0	2.1	2.1	-500	...	004208.5+412409.8	2.2	2.2	2.1	2.1	-300	-330
004208.7+405052.1	2.2	2.1	2.3	2.0	-300	-444	004208.8+412639.9	3.2	2.8	2.9	2.7	-300	...
004208.9+412329.8 <sup>a</sup>	2.3	2.7	2.2	2.1	-300	-335	004209.0+412442.3	2.3	2.3	2.3	2.3	-300	-291
004209.5+412705.5	2.1	2.4	2.3	2.0	-300	...	004209.5+412832.3	3.3	2.9	3.1	2.6	-300	...

Table 1 *continued*

Table 1 (*continued*)

Object	H <sub>2</sub> O	NH <sub>3</sub>	NH <sub>3</sub>	H66 $\alpha$	V <sub>obs</sub>	V <sub>CO</sub>	Object	H <sub>2</sub> O	NH <sub>3</sub>	NH <sub>3</sub>	H66 $\alpha$	V <sub>obs</sub>	V <sub>CO</sub>
(J2000)	(mJy)	(1,1)	(2,2)	(mJy)	(km s <sup>-1</sup> )	(km s <sup>-1</sup> )	(J2000)	(mJy)	(1,1)	(2,2)	(mJy)	(km s <sup>-1</sup> )	(km s <sup>-1</sup> )
004209.8+412412.2	2.2	2.3	2.2	2.3	-300	-331	004210.3+412529.3	2.1	2.7	2.4	2.5	-300	-345
004210.7+412322.3 <sup>a</sup>	2.2	2.0	2.3	2.4	-300	-302	004211.2+412442.6	2.4	2.1	2.3	2.3	-300	-295
004211.6+411909.4	2.7	2.8	2.4	2.6	-300	...	004212.3+412415.7	2.9	2.7	2.7	2.6	-300	-330
004213.8+405117.7	3.9	3.4	3.7	3.5	-300	-406	004214.8+412508.9	2.8	3.0	2.8	2.6	-300	-316
004218.1+412631.1	2.4	2.1	2.6	2.5	-300	-274	004218.7+412751.8	2.7	2.7	2.5	2.6	-300	-330
004220.6+412749.0	3.1	2.6	2.6	2.7	-300	-321	004221.7+412827.6	2.8	4.0	3.2	2.7	-300	-263
004224.8+412758.7	2.9	3.0	3.0	2.8	-300	-307	004225.9+412831.9	2.9	2.7	2.7	2.9	-300	-302
004226.1+410548.2 <sup>a</sup>	3.8	3.0	2.9	2.9	-500	-494	004226.4+412811.2	3.4	2.5	2.3	3.1	-300	-290
004227.6+412019.6	2.1	2.3	2.1	2.0	-300	-226	004227.9+413258.5 <sup>a</sup>	2.5	2.7	2.7	2.5	-300	...
004228.1+405657.7 <sup>a</sup>	2.7	2.3	2.4	2.3	-300	-427	004228.3+412911.4 <sup>a</sup>	3.1	2.9	2.6	3.1	-300	-297
004228.4+412852.4 <sup>a</sup>	1.2	1.3	1.5	1.4	-300	-285	004229.8+410550.6	2.9	2.6	2.5	2.6	-300	...
004230.1+412904.0 <sup>a</sup>	2.8	2.5	2.6	2.6	-300	-282	004230.3+412935.9	4.0	3.0	3.2	3.3	-300	-277
004230.9+405714.6 <sup>a</sup>	3.0	2.8	2.9	3.2	-300	-396	004232.1+412936.5	2.6	2.5	2.5	2.5	-300	-264
004232.3+413008.7	2.7	2.4	2.7	2.6	-300	-277	004232.7+411143.6	2.0	2.1	2.1	2.1	-300	...
004234.2+413007.3	3.0	2.4	3.0	2.6	-300	-267	004235.0+404838.1	2.2	2.3	2.4	2.2	-300	...
004235.3+413224.4	2.4	2.6	2.5	2.7	-300	-265	004235.6+413149.0	3.2	2.8	2.6	2.8	-300	-316
004236.4+413308.7	2.6	2.6	2.5	2.7	-300	-245	004236.9+410158.0	2.5	2.4	2.4	2.4	-300	-419
004237.4+414158.3 <sup>a</sup>	1.8	2.1	2.1	2.3	-300	...	004238.6+413150.5	3.7	2.9	2.9	2.8	-300	-268
004238.9+413135.6	2.9	2.9	2.6	3.3	-300	-276	004240.1+410222.7	3.5	2.8	2.7	2.6	-300	-458
004240.9+405910.8	2.4	2.6	2.4	2.3	-300	-367	004241.3+412246.7	4.1	3.1	3.2	3.4	-300	...
004241.7+411435.0 <sup>a</sup>	3.4	4.0	3.8	3.5	-300	...	004241.7+413245.4	2.5	2.7	2.5	2.5	-300	-265
004241.9+405155.2 <sup>a</sup>	3.6	3.3	3.5	3.7	-300	...	004242.1+410303.0	2.7	2.4	2.7	2.5	-300	-348
004242.5+410001.4	3.0	3.0	2.9	3.2	-300	-372	004242.5+413155.2	3.9	3.2	3.4	3.3	-300	-266
004242.6+411722.5 <sup>a</sup>	4.0	3.7	3.6	3.3	-300	...	004242.9+413159.8	3.7	3.6	3.6	3.8	-300	-269
004244.1+413259.2	3.4	2.5	2.9	2.9	-300	-258	004244.4+411608.5 <sup>a</sup>	3.7	3.4	3.2	3.6	-300	...
004244.9+413338.6	2.3	2.7	2.7	2.5	-300	-245	004245.0+405448.3	2.2	2.3	2.6	2.5	-300	...
004245.2+413316.7	2.6	2.6	2.6	2.6	-300	-257	004245.3+411656.9 <sup>a</sup>	3.6	3.6	3.8	4.0	-300	...
004246.2+410111.4	2.4	2.3	2.4	2.1	-300	-428	004246.8+414447.0	2.2	2.1	2.0	2.0	-300	...
004247.0+411618.4 <sup>a</sup>	3.8	3.9	3.7	3.9	-300	...	004247.0+413333.0	4.0	3.1	3.3	3.1	-300	-248
004247.5+413131.1	2.6	2.4	2.5	2.5	-300	...	004247.9+413400.5	3.1	3.0	3.1	2.9	-300	-254
004248.2+411651.7 <sup>a</sup>	3.6	3.9	4.0	3.6	-300	...	004249.1+411554.6 <sup>a</sup>	3.8	3.6	4.0	3.5	-300	...
004249.1+411945.9 <sup>a</sup>	3.1	2.8	2.4	2.6	-300	...	004249.1+413440.0	2.3	2.7	2.6	2.5	-300	-244
004249.3+412507.5	3.2	2.6	2.7	2.7	-300	-171	004251.0+413507.8	3.2	2.6	3.0	3.0	-300	-242
004252.3+410014.8	2.1	2.0	2.0	1.9	-300	...	004252.4+410120.7	2.8	2.9	2.9	2.4	-300	-331
004253.0+413526.7	2.6	2.4	2.4	2.4	-300	-251	004253.5+413516.2	2.4	2.4	2.3	2.3	-300	-254
004254.4+405832.8	2.3	2.4	2.6	3.0	-300	...	004256.9+413728.1	1.6	1.7	1.8	1.4	-300	-304
004258.2+410015.9	3.1	2.5	2.5	2.8	-300	...	004258.8+413456.2	1.9	2.0	2.0	2.0	-300	-212
004259.1+413741.3	1.9	2.2	2.1	1.9	-300	-268	004259.4+413722.5	2.0	2.2	2.2	1.8	-300	-273
004259.4+413732.1	2.0	2.1	2.1	1.8	-300	-265	004300.0+413526.2	2.0	2.0	2.1	1.9	-300	-184
004300.0+413654.2	2.5	2.4	2.3	2.1	-300	-248	004301.0+413627.9	1.4	1.3	1.3	1.2	-300	-248
004301.5+413717.2	2.8	2.6	2.7	2.6	-300	-244	004301.9+413655.2	1.8	2.1	2.2	1.9	-300	-234
004302.5+413740.5	3.5	3.3	3.2	3.7	-300	-241	004302.5+414910.5	2.1	2.0	2.2	2.0	-300	...
004303.4+413719.3	1.8	2.0	2.0	1.8	-300	-245	004304.3+413739.5	2.0	2.3	2.2	1.9	-300	-232
004304.8+410554.0	2.7	2.3	2.6	2.5	-300	-374	004305.7+413749.8	2.0	1.9	1.8	1.9	-300	-220
004306.7+410213.4	2.2	2.4	2.4	2.4	-300	...	004306.9+413807.1	3.3	2.6	2.8	2.9	-300	-170
004308.2+410156.8	1.3	1.5	1.5	1.5	-300	...	004309.7+413849.3	1.8	1.9	2.3	2.1	-300	-216
004310.0+413751.6 <sup>b</sup>	1.8	2.0	2.0	2.0	-300	-226	004310.5+410426.8	2.3	2.4	2.6	2.6	-300	...
004311.1+413743.3	1.8	2.2	2.1	2.2	-300	-174	004311.3+410459.5	3.6	3.3	3.5	3.7	-300	-380
004311.6+411245.5	2.5	2.4	2.3	2.9	-300	...	004312.4+410125.2	2.3	2.6	2.5	2.3	-300	...

Table 1 *continued*

Table 1 (*continued*)

Object	H <sub>2</sub> O	NH <sub>3</sub>	NH <sub>3</sub>	H66 $\alpha$	V <sub>obs</sub>	V <sub>CO</sub>	Object	H <sub>2</sub> O	NH <sub>3</sub>	NH <sub>3</sub>	H66 $\alpha$	V <sub>obs</sub>	V <sub>CO</sub>
(J2000)	(mJy)	(1,1)	(2,2)	(mJy)	(km s <sup>-1</sup> )	(km s <sup>-1</sup> )	(J2000)	(mJy)	(1,1)	(2,2)	(mJy)	(km s <sup>-1</sup> )	(km s <sup>-1</sup> )
004312.5+413747.4	1.8	2.1	2.0	2.0	-300	...	004312.7+410531.5	1.2	1.3	1.3	1.4	-300	-319
004313.2+410632.4	2.3	2.5	2.3	2.6	-300	-339	004314.0+413906.3	1.9	2.5	2.4	1.9	-300	...
004314.2+410033.9 <sup>a</sup>	2.4	2.3	2.3	2.3	-300	...	004315.2+414947.4	2.0	2.6	2.4	2.3	-300	...
004317.9+410252.8	1.5	1.4	1.4	1.5	-300	...	004320.1+410611.1	1.4	1.2	1.2	1.3	-300	-328
004320.8+414038.5	2.1	2.3	2.2	2.1	-300	-224	004321.7+414033.2	2.3	2.3	2.2	2.5	-300	-261
004322.0+414116.5	2.1	2.2	2.1	2.0	-300	-193	004324.1+414124.7	2.0	1.6	1.8	1.8	-300	...
004324.3+414418.7	1.9	1.7	1.7	1.9	-300	...	004324.4+410802.9	2.5	2.4	2.3	2.1	-300	-312
004325.6+410206.4 <sup>a</sup>	4.4	3.8	3.2	3.9	-300	...	004326.4+410508.4	2.4	2.3	2.3	2.1	-300	...
004328.2+414122.1	1.6	1.8	1.9	2.1	-300	...	004328.6+411818.0	3.9	4.0	3.9	3.9	-300	-299
004329.2+414848.0 <sup>b</sup>	1.2	1.4	1.5	1.4	-300	-226	004330.4+412757.0	2.6	2.6	2.5	2.3	-100	...
004330.4+414432.5	2.4	2.2	2.1	2.4	-300	-231	004331.2+414222.9	2.1	2.2	2.2	2.0	-300	-215
004331.3+414243.6	1.8	2.0	1.9	2.2	-300	-248	004332.1+414251.8	1.2	1.2	1.3	1.5	-300	-242
004332.4+414227.5	1.7	1.7	1.9	2.0	-300	-211	004332.5+410907.0 <sup>a</sup>	2.6	3.1	2.7	2.7	-300	-320
004333.6+411432.3	2.8	2.7	2.4	2.7	-300	-306	004334.9+410953.6	3.8	3.2	3.4	3.9	-300	-308
004338.7+411222.1	2.4	2.6	2.6	2.7	-300	-243	004339.1+411018.4	2.5	2.5	2.8	3.1	-300	-315
004339.3+411001.1	2.8	2.9	2.7	2.6	-300	-306	004339.4+412229.2 <sup>a</sup>	2.3	2.3	2.3	2.3	-300	...
004339.7+414534.9	2.0	2.3	2.1	2.3	-300	...	004340.8+411152.7	2.6	2.4	2.7	2.6	-300	-280
004341.5+414224.3 <sup>a</sup>	2.5	2.5	2.6	2.2	-300	...	004341.6+411135.3	2.8	2.5	2.5	2.5	-300	-307
004341.7+412302.9	2.5	2.7	2.6	2.3	-300	-173	004341.7+414519.4	2.0	1.6	1.6	1.7	-300	-156
004341.7+415313.0 <sup>a</sup>	2.0	2.4	2.2	2.0	-300	...	004343.4+414521.6	2.1	2.1	2.3	2.2	-300	-142
<b>004343.9+411137.6</b>	1.3	1.2	1.4	1.1	-300	-295	004344.6+412321.3	2.4	2.4	2.4	2.6	-300	-168
004346.3+414418.5	3.8	3.3	3.3	3.5	-300	-194	004346.8+411239.7	2.9	2.6	2.4	2.7	-300	-262
004348.1+411133.2	3.2	2.9	3.0	3.0	-300	-297	004349.0+415657.7	3.6	4.1	4.1	4.1	-300	-246
004349.4+411053.8	2.4	2.2	2.1	2.1	-300	...	004351.4+414706.2	3.5	3.7	3.8	4.0	-300	...
004351.4+415718.7	2.1	2.4	2.4	1.9	-300	...	004352.5+412524.1	2.8	2.6	2.7	3.1	-100	-184
004352.5+414858.8	2.3	2.4	2.5	2.1	-300	...	004353.9+415743.8	1.8	2.2	2.2	2.0	-300	...
004354.8+414715.6	2.9	2.5	2.6	2.5	-300	...	004354.9+412603.6	3.2	2.4	2.7	2.7	-100	-154
004355.1+411433.1	2.4	2.2	2.4	2.4	-300	...	004355.2+412650.8	3.0	3.2	2.8	2.8	-100	-169
004355.8+411211.6 <sup>b</sup>	4.1	3.5	3.0	3.9	-300	-249	004356.6+412629.6	2.4	2.1	2.0	1.8	-100	-145
004356.8+414831.6	3.6	3.4	3.5	3.8	-300	-169	004357.7+414854.0	3.1	2.6	2.8	2.6	-300	-154
004358.2+414726.9	3.0	2.3	2.6	2.3	-300	...	004358.7+414837.5	3.0	2.5	2.6	2.4	-300	-116
004358.9+411742.1	2.6	2.4	2.5	2.1	-300	-291	004401.5+414909.6	3.8	3.6	3.6	3.3	-300	-166
004403.0+414954.7	3.1	2.9	2.8	2.4	-300	-168	004403.4+411708.2	2.2	2.3	2.3	2.5	-300	-291
004403.9+413414.8 <sup>a</sup>	3.4	2.7	2.8	2.6	-100	...	004404.2+412107.8	2.5	2.3	2.2	2.6	-300	-266
004404.9+415016.1	2.8	2.7	2.6	2.9	-300	-181	004405.2+412718.2	2.8	2.4	2.8	2.9	-100	-128
004405.7+411719.7	2.3	2.9	2.5	2.4	-300	-255	004406.4+412745.0	2.9	2.6	2.8	2.4	-100	-141
004407.0+412759.3	3.3	2.8	3.0	3.0	-100	-144	004407.8+412110.7	3.0	2.7	2.7	2.6	-300	-248
004409.2+413331.9	2.4	2.3	2.3	2.3	-100	-92	<b>004409.5+411856.6</b>	1.2	1.3	1.3	1.3	-300	-254
004410.5+420247.5 <sup>a</sup>	2.9	2.7	3.0	2.6	-100	...	004410.6+411653.4	2.2	2.4	2.4	2.3	-300	...
004411.0+413206.3	2.1	2.4	2.5	2.5	-100	-127	004411.8+414747.5	2.2	2.3	2.1	1.8	-100	...
004411.9+413356.4	2.1	2.3	2.2	2.3	-100	-80	004412.1+413320.5	2.8	3.1	2.7	2.8	-100	-103
004413.7+413413.5	2.2	2.2	2.4	2.2	-100	-80	004414.4+411742.3	2.4	2.7	2.4	2.3	-300	-266
004414.6+412840.3	2.3	2.5	2.5	2.7	-100	-113	004415.3+411905.7	2.9	2.5	3.8	2.7	-300	-236
004415.9+411717.6	2.1	2.2	2.4	2.2	-300	-252	004416.0+414950.7	3.1	2.7	3.0	2.7	-100	...
004416.1+412105.4	2.3	2.4	2.5	2.2	-300	-244	004416.3+411730.9	2.4	2.6	2.4	2.4	-300	-182
004416.7+412444.1	2.1	2.3	2.2	2.1	-300	-277	004418.2+413406.6	2.8	2.8	2.8	2.8	-100	-152
004419.2+411930.9	2.9	2.5	2.5	2.7	-300	-242	004419.3+412247.0	2.4	2.6	2.5	2.5	-300	-275
004419.9+412201.2	3.2	2.7	2.5	2.7	-300	-272	004420.2+415101.5	3.4	2.5	2.6	2.8	-100	...
004420.7+411751.0	2.3	2.6	2.7	2.2	-300	...	004420.9+411835.7	2.5	2.5	2.5	2.4	-300	-254

Table 1 *continued*

Table 1 (*continued*)

Object	H <sub>2</sub> O	NH <sub>3</sub>	NH <sub>3</sub>	H66 $\alpha$	V <sub>obs</sub>	V <sub>CO</sub>	Object	H <sub>2</sub> O	NH <sub>3</sub>	NH <sub>3</sub>	H66 $\alpha$	V <sub>obs</sub>	V <sub>CO</sub>
(J2000)	(mJy)	(1,1)	(2,2)	(mJy)	(km s <sup>-1</sup> )	(km s <sup>-1</sup> )	(J2000)	(mJy)	(1,1)	(2,2)	(mJy)	(km s <sup>-1</sup> )	(km s <sup>-1</sup> )
004422.8+412529.1	2.1	2.3	2.2	2.1	-300	...	004423.0+412050.9	3.3	2.9	3.0	2.7	-300	-245
004423.3+413842.6	2.8	2.6	3.0	2.7	-100	...	004423.7+412437.3	3.3	2.5	2.5	2.6	-300	-233
004424.1+412117.3	2.9	2.8	2.7	2.9	-300	-218	004424.2+414918.9	3.2	2.4	2.5	2.7	-100	-102
004424.4+415120.5	1.7	2.0	2.1	2.0	-100	-164	004424.9+413739.1	2.1	2.1	1.9	1.8	-100	-66
004425.0+414942.6	1.8	2.2	2.1	1.9	-100	...	004425.4+415006.1	1.8	2.2	2.1	2.1	-100	...
004426.2+412054.1	2.4	2.1	2.1	2.0	-300	-226	004426.7+412729.3	2.4	2.3	2.2	2.2	-300	-217
004427.5+413529.8	3.0	2.5	2.7	2.5	-100	...	004429.1+412334.0	3.2	2.5	2.8	2.6	-300	-228
004429.6+412138.9	2.1	2.1	2.1	2.2	-300	-268	004429.6+415133.5	1.9	2.0	1.9	2.0	-100	-113
004430.2+415242.7	2.0	2.1	2.3	2.0	-100	-107	<b>004430.5+415154.8</b>	1.1	1.1	1.1	1.2	-100	-96
004431.1+415110.2	3.0	2.6	2.9	3.0	-100	-104	004431.1+415638.2	1.9	2.0	2.1	1.9	-100	-94
004431.9+412233.3	2.9	2.6	2.7	2.6	-300	-196	004431.9+412400.1	2.2	2.2	2.0	4.5	-300	-219
004432.6+412518.7	2.2	2.3	2.3	2.4	-300	-172	004433.8+415249.7 <sup>b</sup>	2.3	2.1	1.9	2.1	-100	-90
004435.6+415606.9 <sup>b</sup>	3.1	2.6	2.6	2.8	-100	...	004436.7+412445.1	2.3	2.9	2.6	2.5	-300	-189
004437.3+415350.2	1.9	2.1	2.3	1.9	-100	...	004437.7+415259.8	2.1	2.4	2.3	2.4	-100	-101
004437.9+415154.0	3.8	2.5	2.7	2.6	-100	-137	004438.5+412511.1	3.7	3.4	3.3	3.6	-300	-211
004439.4+415251.3	2.2	2.4	2.2	2.3	-100	-107	004440.3+414923.9	1.9	2.2	2.2	2.0	-100	...
004441.5+415312.7	1.9	2.0	2.2	1.9	-100	-103	004441.7+412659.6	2.1	2.4	2.1	2.2	-300	-208
004442.7+415341.1	1.3	1.4	1.4	1.3	-100	-98	004443.9+412758.0	3.9	3.3	3.9	3.6	-300	-186
004444.1+415359.0	3.3	2.5	2.6	2.7	-100	-59	004444.8+412839.9	2.6	2.4	2.6	2.6	-300	-165
004447.1+415657.7	2.5	2.5	2.3	2.2	-100	...	004447.6+412641.5	2.5	2.5	2.5	2.5	-300	...
004448.1+415307.3	2.3	2.5	2.4	2.4	-100	-91	004448.4+412254.2	3.1	3.0	2.9	2.7	-300	...
004448.6+415343.6	2.3	2.5	2.5	2.3	-100	-87	004450.6+415608.3	2.3	2.3	2.3	2.0	-100	-42
004450.9+412909.2	2.2	2.4	2.3	2.3	-300	-179	004451.8+415423.7	1.2	1.3	1.4	1.3	-100	-131
004452.7+415309.1	1.3	1.5	1.4	1.5	-100	-62	004452.8+415457.5	2.3	2.1	2.0	2.3	-100	-95
004453.0+415340.3	3.0	2.9	2.8	3.0	-100	-101	004454.4+420327.4	1.8	2.0	2.2	2.1	-100	...
004456.1+412918.2	3.2	2.9	2.8	2.7	-300	-174	004456.2+413124.1	2.5	2.3	2.0	2.1	-300	-153
004457.2+415524.0	3.1	2.7	2.6	2.6	-100	-72	004457.3+413141.8	2.1	2.4	2.4	1.9	-300	...
004458.0+414034.7	1.3	1.6	1.4	1.3	-100	...	004458.1+420008.6	2.3	2.2	2.3	2.3	-100	-114
004458.3+415906.9	2.4	2.4	2.4	2.2	-100	...	004458.7+415536.1	2.1	1.9	1.7	3.2	-100	-81
004459.1+413233.8	4.2	3.3	4.8	3.3	-300	-166	004459.1+414058.5	3.1	2.7	2.8	2.9	-100	...
004459.3+413139.2	2.9	2.2	2.4	2.5	-300	-180	004459.5+415510.4	2.4	2.6	2.3	2.4	-100	-68
004500.7+412836.9	4.1	3.2	3.3	3.4	-300	-191	004500.9+413101.1	3.0	2.8	2.8	2.9	-300	...
004503.0+413249.4	2.0	2.3	2.1	1.9	-300	-153	004504.6+413237.6	1.8	2.1	2.4	2.0	-300	-151
004505.3+413845.9	2.3	2.5	2.4	2.7	-100	...	004505.9+413925.5	2.2	2.4	2.3	2.3	-100	-126
004506.1+413615.0	2.1	1.9	1.9	1.8	-100	-154	004506.1+415121.0	3.4	2.7	3.8	2.6	-100	-52
004506.2+413424.4	3.0	2.6	2.6	2.7	-100	-150	004506.9+413407.8	2.8	2.7	2.7	2.7	-100	-140
004507.5+413439.4	2.1	2.4	2.4	2.4	-100	-144	004508.2+413424.2	2.2	2.5	2.3	2.4	-100	-132
004509.0+415209.7	3.3	2.7	2.6	2.7	-100	-62	004510.0+420143.6	2.3	2.7	2.4	2.5	-100	...
004510.3+420228.5	2.6	2.5	2.5	2.6	-100	...	004510.4+413716.0	1.9	2.2	2.2	2.1	-100	-104
004510.5+413426.7	2.4	2.4	2.2	2.5	-100	-121	004510.8+415938.9	2.3	2.3	2.2	2.1	-100	...
004511.2+413644.9	3.3	2.7	2.5	2.6	-100	-116	004511.3+413633.9	2.7	2.7	2.9	2.6	-100	-136
004511.6+420130.3	2.0	2.1	2.4	2.1	-100	...	004512.1+415542.5	1.9	2.0	2.2	2.0	-100	-55
004512.4+413709.6	3.2	2.7	2.8	2.6	-100	-129	004512.8+413531.6	2.4	1.9	2.1	2.0	-100	-133
004514.4+413723.6	2.5	2.4	2.3	2.6	-100	-120	004515.2+413948.5	3.1	2.5	2.6	2.5	-100	...
004515.9+420254.4 <sup>a</sup>	2.3	2.4	2.3	2.3	-100	...	004518.1+413920.5	2.2	2.5	2.6	2.2	-100	-86
004518.5+414013.2	2.1	2.1	2.1	1.8	-100	...	004518.7+413906.1	2.2	2.1	2.4	2.2	-100	...
004518.8+420331.8	1.2	1.4	1.3	1.5	-100	...	004520.7+414716.7	3.1	2.5	2.8	2.5	-100	-100
004520.9+414248.8	2.3	2.2	2.3	1.9	-100	...	004521.6+420345.1	2.3	2.3	2.4	2.3	-100	...
004523.1+414346.0	2.0	2.0	2.1	2.3	-100	-103	004524.4+415537.4	2.1	1.8	2.1	3.6	-100	...

Table 1 *continued*



Table 1 (*continued*)

Object (J2000)	H <sub>2</sub> O (mJy)	NH <sub>3</sub> (1,1) (mJy)	NH <sub>3</sub> (2,2) (mJy)	H66 $\alpha$ (mJy)	V <sub>obs</sub> (km s <sup>-1</sup> )	V <sub>CO</sub> (km s <sup>-1</sup> )	Object (J2000)	H <sub>2</sub> O (mJy)	NH <sub>3</sub> (1,1) (mJy)	NH <sub>3</sub> (2,2) (mJy)	H66 $\alpha$ (mJy)	V <sub>obs</sub> (km s <sup>-1</sup> )	V <sub>CO</sub> (km s <sup>-1</sup> )
004526.8+415820.1	2.6	2.0	2.1	2.6	-100	...	004527.0+415135.5	1.8	2.4	2.2	2.0	-100	...
004528.0+415928.1	2.6	2.6	2.3	2.3	-100	-50	004528.2+414513.6	3.1	2.8	2.4	2.8	-100	-91
004528.2+414630.6	1.7	2.1	2.3	2.1	-100	-75	004528.6+415000.2	2.1	2.0	2.3	2.0	-100	-55
004532.2+414543.3	2.0	2.5	2.2	1.9	-100	-94	004533.3+414739.8	2.0	2.4	2.3	2.1	-100	-61
004533.6+414728.2	2.3	2.3	2.4	2.5	-100	-70	004534.1+414703.3	2.3	2.5	2.2	2.5	-100	...
004536.3+414252.0	2.1	2.3	2.3	2.4	-100	-129	004536.5+415307.7	2.2	2.0	2.2	2.0	-100	-78
004536.9+415704.0	3.2	2.7	2.7	2.4	-100	-72	004537.2+415802.4	2.9	2.6	2.8	3.0	-100	-36
004537.3+415107.0	3.2	2.9	2.7	2.6	-100	...	004537.6+415424.1	3.2	2.8	3.1	2.8	-100	-67
004538.5+415231.1	3.2	2.9	2.9	2.4	-100	-45	004540.0+415510.2 <sup>b</sup>	3.2	2.7	2.5	2.9	-100	-63
004541.4+415550.4	1.9	2.0	2.0	2.2	-100	-59	004541.6+415107.7	3.3	2.5	2.6	2.6	-100	-89
004542.9+415234.8	2.5	2.0	2.0	2.0	-100	-62	004543.3+415109.3	1.1	1.2	1.2	1.2	-100	...
004543.3+415301.1	3.0	2.7	2.6	2.7	-100	-57	004543.5+414235.1	2.0	2.3	2.0	2.0	-100	...
004544.3+415207.4	3.1	2.9	2.8	2.8	-100	-31	004549.7+421017.1	2.3	2.3	2.4	2.0	-100	...
004555.2+415645.8	2.1	2.2	2.5	2.1	-100	...	004608.5+421131.0	2.9	2.6	3.0	2.7	-100	...
004613.4+415224.4	2.1	2.5	2.4	2.2	-100	...	004617.6+415158.0	3.4	2.7	2.7	2.8	-100	-122
004623.9+421215.2	2.1	2.4	2.5	2.5	-100	...	004625.4+421156.0	2.2	2.3	2.3	2.3	-100	...
004626.0+421121.7	2.2	2.3	2.2	2.3	-100	...	004627.9+415920.4	2.2	2.4	2.3	2.2	-100	...
004631.5+421342.6	2.4	2.5	2.4	2.3	-100	...	004633.4+421244.2	2.5	2.3	2.4	2.2	-100	...
004633.6+415932.0	3.0	2.8	2.8	2.8	-100	...	004634.2+415636.8	1.9	2.1	2.2	2.1	-100	...
004634.4+421143.1	2.4	2.0	2.0	1.9	-100	...	004641.6+421156.2 <sup>b</sup>	3.2	2.7	2.7	2.6	-100	...
004641.9+421547.8	2.3	2.4	2.5	2.4	-100	...	004642.2+415837.3	2.4	2.5	2.3	2.3	-100	...
004642.6+421406.8 <sup>a</sup>	2.4	2.5	2.5	2.6	-100	...	004645.9+420453.1	2.2	2.2	2.3	2.3	-100	...
004654.5+420046.2	2.3	2.2	2.6	2.2	-100	...	004703.1+415755.4 <sup>a</sup>	2.3	2.3	2.5	2.3	-100	...

<sup>a</sup> Giant star identified by Amiri & Darling (2016).

<sup>b</sup> Planetary nebula identified by Merrett et al. (2006).

NOTE—Detected H<sub>2</sub>O maser regions are in bold. The rms noise is quoted per 3.1–3.3 km s<sup>-1</sup> (244 kHz) channels. V<sub>obs</sub> is the observed central velocity tuning of the 632–674 km s<sup>-1</sup> (50 MHz) bandwidth. V<sub>CO</sub> uncertainties are typically ~1 km s<sup>-1</sup> (Nielen et al. 2006), but the CO velocity map shows mean and median dispersions of 19 and 13 km s<sup>-1</sup> within the GBT beam. All velocities are in the heliocentric reference frame using the optical definition.

Observations were conducted with the dual K-band receivers in 2010 and beams 1 and 2 of the K-band focal plane array in 2011–2012 in a nodding mode in two circular polarizations with 0.15–0.16 km s<sup>-1</sup> (12.2 kHz) channels and 9-level sampling. The time on-source was 5 minutes except for sources that were re-observed to confirm or refute possible lines (typically 10 minutes). A winking calibration diode and hourly atmospheric opacity estimates were used for flux density calibration. Opacities ranged from 0.03 to 0.14 neper but were typically 0.06 neper. The estimated uncertainty in the flux density calibration is ~20%. Pointing and focus corrections were made hourly. Pointing was typically good to within a few arcseconds, and the largest pointing corrections during observing sessions were no more than 6". The resolution of the 24  $\mu$ m Spitzer image is 6" (Gordon et al. 2008), so the unresolved IR sources remained within the 33" GBT beam even during the largest pointing drifts. The 33" beam (FWHM) at 22 GHz spans 125 pc in M31.

After averaging polarizations, spectra were Hanning smoothed and subsequently Gaussian smoothed to obtain a final spectral resolution of 3.1–3.3 km s<sup>-1</sup> (244 kHz) for the line search. H66 $\alpha$  was also smoothed to 9.8 km s<sup>-1</sup> (732 kHz) to search for broad recombination lines (e.g., Dieter 1967; Mezger & Höglund 1967). Polynomial baselines, typically of fifth order, were fit and subtracted to obtain flat and generally uniform-noise spectra. Spectral rms noise measurements for each pointing center and observed line are listed in Table 1. Non-detection spectra generally did not show any features greater than 3 $\sigma$ , corresponding to roughly 10 mJy, at least an order of magnitude more sensitive than previous surveys (Greenhill et al. 1995; Imai et al. 2001, Claussen & Beasley, priv. comm.), and likely the weakest line that can currently be used for VLBI proper motion studies. All data reduction



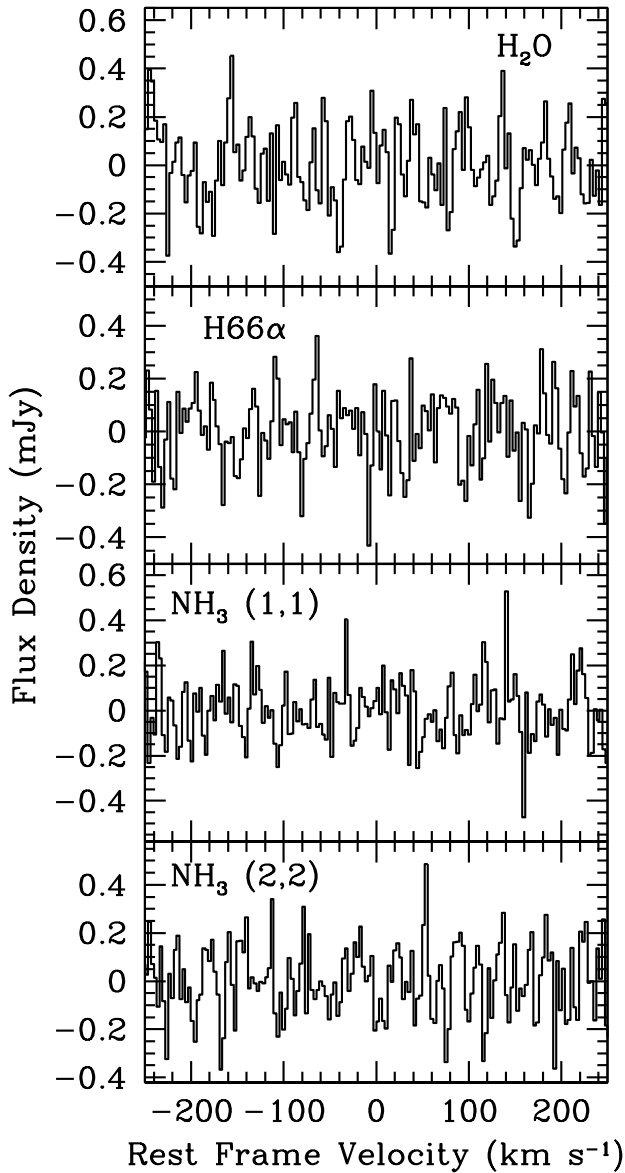


**Figure 2.** Mean stacks of 300 spectra (299 spectra for  $\text{H}_2\text{O}$ ). Velocities of individual spectra were centered on the local CO velocity measured by [Nieten et al. \(2006\)](#) prior to stacking. Channels are  $3.1\text{--}3.3 \text{ km s}^{-1}$ . Median stacks show a similar lack of significant lines and 12–21% higher noise.

was performed in GBTIDL<sup>2</sup>.

In order to assess the average and median line emission of the sample, we aligned  $\text{H}_2\text{O}$ ,  $\text{NH}_3$ , and  $\text{H66}\alpha$  spectra according to the [Nieten et al. \(2006\)](#) CO velocities and median- and mean-stacked them to determine whether the median or mean object selected for the survey produces line emission in a given species an order of magnitude below the single-spectrum sensitivity. Spectra were noise-weighted in the

mean stacks, and 300 spectra were used for both the mean and median stacks (except for the  $\text{H}_2\text{O}$  stacks, which used 299 spectra). Omitted spectra either had no CO velocity information, had unreliable CO velocity information, or have been identified to be other than an H II region (indicated with footnotes in Table 1; see also Section 4). Every object in Table 1 was manually inspected in the [Nieten et al. \(2006\)](#) CO velocity map to ensure that no mask edges, incomplete data, or high (instrumental) velocity dispersion regions were included in the stack. All objects in Table 1 that show a CO velocity can be considered reliable.

#### 4. RESULTS

We have detected water maser emission in five out of 506  $24 \mu\text{m}$ -selected regions in M31 (Table 1). The water maser isotropic line luminosity sensitivity is  $4.4 \times 10^{-4} L_{\odot}$ , which is a  $3\sigma$  peak line flux density limit of 9 mJy and width  $3.3 \text{ km s}^{-1}$ . The detected water masers were presented in [Darling \(2011\)](#) and are not reproduced here. Omitting the 44 objects likely to be planetary nebulae (9 objects; [Merrett et al. 2006](#); [Amiri & Darling 2016](#)) or giant stars (35 objects; [Amiri & Darling 2016](#)), the overall detection rate is 1.1(0.5)%. The actual water maser fraction likely depends on star formation stage and conditions, and our overall detection rate is a strong function of the survey sensitivity; [Amiri & Darling \(2016\)](#) demonstrate that we detect only the high luminosity tail of the underlying maser population. Conversely, it is unlikely that all of the remaining  $24 \mu\text{m}$  sources are compact H II regions (e.g., [Verley et al. 2007](#); [Mould et al. 2008](#)), so the maser fraction among star-forming regions may be higher than 1.1(0.5)% given the survey sensitivity. The maser detection rate would also be higher were we to use a more refined selection method such as the one presented in [Amiri & Darling \(2016\)](#).

No  $\text{NH}_3$  or  $\text{H66}\alpha$  lines were detected in the survey; see Table 1 for rms noise values. Figure 2 shows the noise-weighted mean spectral stacks for the four observed spectral lines:  $\text{H}_2\text{O}$ ,  $\text{H66}\alpha$ ,  $\text{NH}_3 (1,1)$ , and  $\text{NH}_3 (2,2)$ . The stacks of 300 spectra (299 spectra for  $\text{H}_2\text{O}$ ) reached rms noise values of 0.17, 0.14, 0.15, and 0.15 mJy per  $3.1\text{--}3.3 \text{ km s}^{-1}$  channel, respectively. The median stacks appear similar to the mean stacks, but with 12, 21, 20, and 13% higher noise. No lines are detected in these stacks, which show the expected  $\sqrt{N}$  noise improvement over single-object spectra.

#### 5. DISCUSSION

Neither the mean nor the median compact  $24 \mu\text{m}$ -emitting region selected for the water maser survey shows detectable emission in the four observed lines. In all of the stacked spectra, errors in the CO velocity used to center spectra, CO velocity variance, and CO line peak offsets from the denser molecular gas velocity, can all contribute to incorrect spectral shifts in the stacking process. These factors will dilute the detectability of lines in spectral stacks, particularly in the

<sup>2</sup> GBTIDL (<http://gbtidl.nrao.edu/>) is the data reduction package produced by NRAO and written in the IDL language for the reduction of GBT data.

mean.

The water maser fraction in Galactic surveys can be of order 50% (e.g., Kurtz & Hofner 2005; Urquhart et al. 2011), so one might expect to detect line emission from the median object in an adequately deep survey. While the line luminosity sensitivity of the M31 survey does not reach the sensitivity needed in Galactic surveys to detect the median water maser in individual spectra, the median spectral stack reaches a  $3\sigma$  luminosity sensitivity of  $2.8 \times 10^{-5} L_{\odot}$  (assuming a  $3.3 \text{ km s}^{-1}$ -wide maser). Since the median Urquhart et al. (2011)  $\text{H}_2\text{O}$  maser isotropic line luminosity is  $1 \times 10^{-5} L_{\odot}$  and since the CO velocity alignment of the stacks lacks the velocity precision needed for alignment of few  $\text{km s}^{-1}$  lines, the M31 spectral stack cannot quite detect the median Galactic H II water maser equivalent.

For the  $\text{H}66\alpha$  line, the non-detection in stacked spectra probably implies that the mean or median region simply does not emit in this line. Aside from selecting for 22 GHz radio continuum backlights, the  $24 \mu\text{m}$  selection method is sub-optimal for hydrogen radio recombination lines (the  $\text{H}66\alpha$  line was included in the GBT observations to allow serendipitous detection).

$\text{NH}_3$  emission, in contrast, is common in H II regions; Urquhart et al. (2011) obtain a detection rate of  $\sim 80\%$ , fairly independent of H II region luminosity, and Dunham et al. (2011) detected  $\text{NH}_3$  (1,1) toward 72% of 1.1 mm continuum sources in the inner Galaxy. One would expect to detect  $\text{NH}_3$  lines in mean or median spectra of adequate depth, provided the  $\text{NH}_3$  filling factor does not become too small at the distance of M31. We discuss these issues below.

### 5.1. Water Maser Detection Rate and Star Formation

The sensitivity of the GBT survey corresponds to a  $\sim 200 \text{ Jy}$  Galactic maser 6 kpc distant. There are 23  $\text{H}_2\text{O}$  masers in the Palagi et al. (1993) sample and roughly 30 masers in the Breen et al. (2010) sample that our survey could detect at the distance of M31. Hence, sensitivity is not the only consideration; the number of water masers detectable in M31 will also depend on the substantially lower star formation rate of M31 compared to Galactic. The maser detection rate, however, should be comparable between galaxies in similarly-selected samples of star-forming regions if the physical conditions of star formation are similar.

In the Urquhart et al. (2011) Galactic water maser survey, there are 30  $\text{H}_2\text{O}$  masers with peak flux density greater than 200 Jy, and there are 22  $\text{H}_2\text{O}$  masers with isotropic luminosity greater than  $4.4 \times 10^{-4} L_{\odot}$ . Were this Galactic survey restricted to the luminosity sensitivity of the M31 water maser survey, the net detection rate would fall from 52(2)% to 3.7(0.8)%, which is not significantly different from our M31 detection rate of 1.1(0.5)%. The Urquhart et al. (2011) detection rate, however, is a strong function of H II region bolometric luminosity, approaching 100% in the highest luminosity regions. Owing to the order-of-magnitude reduced

star formation rate in M31 compared to the Galaxy, this high luminosity tail of star-forming regions may not exist in M31, further reducing the expected maser detection rate.

To estimate the total number of expected water masers in Local Group galaxies, Brunthaler et al. (2006) used the Greenhill et al. (1990) Galactic water maser luminosity function (LF) scaled from the Galactic star formation rate to that of Local Group galaxies, assuming that maser population is proportional to the star formation rate. Local Group water maser statistics agree fairly well with this approach (Brunthaler et al. 2006). Updating Darling (2011), we scale the Galactic star formation rate of  $\sim 2 M_{\odot} \text{ yr}^{-1}$  (Chomiuk & Povich 2011) to that of M31,  $0.25_{-0.04}^{+0.06} M_{\odot} \text{ yr}^{-1}$  (Ford et al. 2013), to predict 3.3 water masers for an isotropic line luminosity limit of  $4.4 \times 10^{-4} L_{\odot}$ . This prediction suffers from small number statistics, but our five detections suggest that either we have detected the majority of bright water masers in M31 (the high-luminosity tail of the water maser LF) or that the star formation scaling approach is inaccurate. The former seems more likely: Amiri & Darling (2016) show that we have surveyed nearly all of the regions most likely to produce luminous water masers and that there are probably no more bright water masers to be found in M31.

### 5.2. Ammonia

While ammonia lines lack the intrinsic brightness temperature of  $\text{H}_2\text{O}$ , they can be beam-filling. Given the mean  $T_{\text{mb}} = 1.1 \text{ K}$  (1,1) line peak and mean distance of  $\sim 5 \text{ kpc}$  of the Urquhart et al. (2011) sample, and using a GBT main-beam efficiency of 0.87 and gain of  $1.88 \text{ K Jy}^{-1}$  (Mangum et al. 2013), the average Galactic  $\text{NH}_3$  emission from an H II region<sup>3</sup> scaled to the distance of M31 would produce a  $\sim 0.02 \text{ mJy}$  line peak, all other factors being equal and assuming no confusion in the  $\text{NH}_3$  emission from multiple H II regions along Galactic sight lines (the Dunham et al. (2011) measurements provide a similar prediction). There would thus need to be roughly 150 such  $\text{NH}_3$  emitters within a GBT beam to approach the rms noise in a single pointing. The rough size of a Galactic  $\text{NH}_3$  source in the Urquhart et al. (2011) sample is 0.2-0.4 pc, so by area, it is possible that 150 such objects could fall within the 121 pc GBT beam in the molecular ring of M31. The brightest H II region in the Urquhart et al. (2011) sample would appear at 0.13 mJy in M31, still a factor of  $\sim 20$  below the rms noise in individual spectra. The  $\text{NH}_3$  (2,2) line is typically weaker than the (1,1) line, so our observations of the (2,2) line are less constraining than the (1,1) line.

The mean-stacked  $\text{NH}_3$  (1,1) spectra show an rms noise per channel seven times higher than the expected average Galactic  $\text{NH}_3$  (1,1) line emitter, but if the average 121 pc-diameter

<sup>3</sup> Not all  $\text{NH}_3$ -emitting objects in the Urquhart et al. (2011) sample are H II regions.

region contained roughly 20 such regions, then a  $3\sigma$  peak would be detected. The data do not support this.

Extragalactic  $\text{NH}_3$  cm metastable lines have been detected toward numerous galaxies, some down to the few mJy/mK level by, e.g., [Martin & Ho \(1979\)](#); [Takano et al. \(2000\)](#); [Henkel et al. \(2000\)](#); [Weiß et al. \(2001\)](#); [Takano et al. \(2002\)](#); [Mauersberger et al. \(2003\)](#); [Ott et al. \(2005, 2011\)](#), and [Mangum et al. \(2013\)](#), but in most cases the galaxies are actively star-forming — if not starbursts — at substantially higher rates than M31. The non-detection of  $\text{NH}_3$  toward M31 is not yet constraining on the  $\text{NH}_3$  abundance compared to the Galactic value.

## 6. CONCLUSIONS

We have expanded a survey for  $\text{H}_2\text{O}$  masers in M31 based on pointed observations of 24  $\mu\text{m}$ -selected regions. While the 24  $\mu\text{m}$  selection method clearly succeeds in identifying water masers (albeit at the low rate of 1.1(0.5)%), 24  $\mu\text{m}$  emission is a necessary but not a sufficient condition for water maser activity (see [Amiri & Darling \(2016\)](#) for a study of the properties of star-forming regions most likely to produce water masers). In [Darling \(2011\)](#), we suggested that the catalog of water masers in M31 is incomplete and that an exhaustive survey of IR-luminous regions would identify additional masers. The prediction was too optimistic, and it should be noted that the detected masers are consistent with the aggregate star formation rate of M31 given its distance and the sensitivity of the survey. New masers could still be detected in deeper surveys or in future surveys of similar depth, given the variable nature of water masers in star-forming regions. However, variability also implies that the currently detected

masers could themselves be flaring and therefore fade, limiting their astrometric utility.

For now, the five known water masers in M31 will have to serve as the basis for proper motion studies, which will probably minimally constrain the three expected proper motion signals (plus random peculiar maser motions) described by [Darling \(2011\)](#): (1) the systemic proper motion (already constrained by [Sohn et al. 2012](#); [van der Marel et al. 2012a](#)), (2) proper rotation, and (3) proper expansion caused by the  $-300 \text{ km s}^{-1}$  (heliocentric) approach of M31 (see also [Darling 2013](#)). We predict that proper rotation and systemic proper motion will be measurable in a few years with current facilities, and that the “moving cluster” divergence of maser spots as M31 approaches the Galaxy may be detectable in a decade ([Darling 2013](#)), but a possible previous interaction between M31 and M32 may have produced peculiar radial motions in the molecular ring of M31 that would mask this signal ([Block et al. 2006](#); [Dierickx et al. 2014](#)).

All authors acknowledge support from the NSF grant AST-1109078. The authors thank K. Gordon for the Spitzer map, M. Claussen and T. Beasley for sharing their results, and the anonymous referee for helpful comments. This research has made use of NASA’s Astrophysics Data System Bibliographic Services and the NASA/IPAC Extragalactic Database (NED) and uses observations made with the *Spitzer Space Telescope*, both of which are operated by the Jet Propulsion Laboratory, California Institute of Technology, under a contract with NASA.

*Facility:* GBT

## REFERENCES

- Amiri, N. & Darling, J. 2016, ApJ, submitted
- Block, D. L., Bournaud, F., Combes, F., Gross, R., Barmby, P., Ashby, M. L. N., Fazio, G. G., Pahre, M. A., & Willner, S. P. 2006, Nature, 443, 832
- Breen, S. L., Caswell, J. L., Ellingsen, S. P., & Phillips, C. J. 2010, MNRAS, 406, 1487
- Brunthaler, A., Reid, M. J., Falcke, H., Greenhill, M. J., & Henkel, C. 2005, Science, 307, 1440
- Brunthaler, A., Henkel, C., de Blok, W. J. G., Reid, M. J., Greenhill, L. J., & Falcke, H. 2006, A&A, 457, 109
- Brunthaler, A., Reid, M. J., Falcke, H., Henkel, C., & Menten, K. M. 2007, A&A, 462, 101
- Chomiuk, L. & Povich, M. S. 2011, AJ, 142, 197
- Churchwell, E., Witzel, A., Huchtmeier, W., Pauliny-Toth, I., Roland, J., & Sieber, W. 1977, A&A, 54, 969
- Darling, J. 2011, ApJ, 732, L2
- Darling, J. 2013, ApJ, 777, L21
- de Vaucouleurs, G., de Vaucouleurs, A., Corwin, H. G., Jr., Buta, R. J., Paturel, G., & Fouqué, P. 1991, Third Reference Catalogue of Bright Galaxies (New York: Springer)
- Dierickx, M., Blecha, L., & Loeb, A. 2014, ApJ, in press (arXiv:1405.3990)
- Dieter, N. H. 1967, ApJ, 150, 435
- Dunham, M. K., Rosolowsky, E., Evans, N. J., II, Cyganowski, C., & Urquhart, J. S. 2011, ApJ, 741, 110
- Ford, G. P., Gear, W. K., Smith, M. W. L., et al. 2013, ApJ, 769, 55
- Gordon, K. D., et al. 2008, ApJ, 638, L87
- Greenhill, L. J., et al. 1990, ApJ, 364, 513
- Greenhill, L. J., Henkel, C., Becker, R., Wilson, T. L., & Wouterloot, J. G. A. 1995, A&A, 304, 21
- Henkel, C., Wouterloot, J. G. A., & Bally, J. 1986, A&A, 155, 193
- Henkel, C., Mauersberger, R., Peck, A. B., Falcke, H., & Hagiwara, Y. 2000, A&A, 361, L45
- Henkel, C., Peck, A. B., Tarchi, A., Nagar, N. M., Braatz, J. A., Castangia, P., & Moscadelli, L. 2005, A&A, 436, 75
- Imai, H., Ishihara, Y., Kameya, O., & Nakai, N. 2001, PASJ, 53, 489
- Jaffe, D. T., Guesten, R., & Downes, D. 1981, ApJ, 250, 621
- Kurtz, S. & Hofner, P. 2005, AJ, 130 711
- Loeb, A., Reid, M. J., Brunthaler, A., & Falcke, H. 2005, ApJ, 633, 894
- Mangum, J. G., Darling, J., Henkel, C., Menten, K. M., MacGregor, M., Svoboda, B. E., & Schinnerer, E. 2013, ApJ, 779, 33
- Martin, R. N. & Ho, P. T. P. 1979, A&A, 74, L7
- Mauersberger, R., Henkel, C., Weiß, A., Peck, A. B., & Hagiwara, Y. 2003, A&A, 403, 561
- McConnachie, A. W., Irwin, M. J., Ferguson, A. M. N., Ibata, R. A., Lewis, G. F., & Tanvir, N. 2005, MNRAS, 356, 979
- Merrett, H. R., Merrifield, M. R., Douglas, N. G., et al. 2006, MNRAS, 369, 120
- Mezger, P. G., & Höglund, B. 1967, ApJ, 147, 490

- Mould, J., Barmby, P., Gordon, K., Willner, S. P., Ashby, M. L. N., Gehrz, R. D., Humphreys, R., & Woodward, C. E. 2008, *ApJ*, 687, 230
- Nieten, C., Neininger, N., Guélin, M., Ungerechts, H., Lucas, R., Berkhuijsen, E. M., Beck, R., & Wielebinski, R. 2006, *A&A*, 453, 459
- Ott, J., Weiß, A., Henkel, C., & Walter, F. 2005, *ApJ*, 629, 767
- Ott, J., Henkel, C., Braatz, J. A., & Weiß, A. 2011, *ApJ*, 742, 95
- Palagi, F., Cesaroni, R., Comoretto, G., Felli, M., & Natale, V. 1993, *A&A*, 101, 15
- Peebles, P.J.E., Phelps, S.D., Shaya, E.J., & Tully, R.B. 2001, *ApJ*, 554, 104
- Reid, M. J., Brunthaler, A., Menten, K. M., Loinard, L., & Wrobel, J. 2009, *Astro2010*, 2010, 243
- Sjouwerman, L. O., Murray, C. E., Pihlstrom, Y. M., Fish, V. L., & Araya, E. D. 2010, *ApJ*, 724, L158
- Sohn, S. T., Anderson, J., & van der Marel, R. P. 2012, *ApJ*, 753, 7
- Sullivan, W. T., III. 1973, *ApJS*, 25, 393
- Tabatabaei, F. S. & Berkhuijsen, E. M. 2010, *A&A*, 517, 77
- Takano, S., Nakai, N., Kawaguchi, K., & Takano, T. 2000, *PASJ*, 52, L67
- Takano, S., Nakai, N., & Kawaguchi, K. 2002, *PASJ*, 54, 195
- Urquhart, J. S., Morgan, L. K., Figura, C. C., Moore, T. J. T., Lumsden, S. L., Hoare, M. G., Oudmaijer, R. D., Mottram, J. C., Davies, B., & Dunham, M. K. 2011, *MNRAS*, 418 1689
- van der Marel, R. P., Fardal, M., Besla, G., Beaton, R. L., Sohn, S. T., Anderson, J., Brown, T., & Guhathakurta, P. 2012, *ApJ*, 753, 8
- van der Marel, R. P., Besla, G., Cox, T. J., Sohn, S. T., & Anderson, J. 2012, *ApJ*, 753, 9
- Verley, S., Hunt, L. K., Corbelli, E., & Giovanardi, C. 2007, *A&A*, 476, 1161
- Weiß, A., Neininger, N., Henkel, C., Stutzki, J., & Klein, U. 2001, *ApJ*, 554, L143